

# ShaRPy: Shape Reconstruction and Hand Pose Estimation from RGB-D with Uncertainty

Vanessa Wirth<sup>1</sup>, Anna-Maria Liphardt<sup>1,2,3</sup>, Birte Coppers<sup>1,2,3</sup>, Johanna Bräunig<sup>1</sup>, Simon Heinrich<sup>1</sup>, Arnd Kleyer<sup>1,2,3</sup>, Georg Schett<sup>1,2,3</sup>, Martin Vossiek<sup>1</sup>, Bernhard Egger<sup>1</sup>, and Marc Stamminger<sup>1</sup>

<sup>1</sup> Friedrich-Alexander-Universität (FAU) Erlangen-Nürnberg, Germany

<sup>2</sup> Department of Internal Medicine 3 - Rheumatology and Immunology, Universitätsklinikum Erlangen, FAU Erlangen-Nürnberg, Germany

<sup>3</sup> Deutsches Zentrum Immuntherapie, Universitätsklinikum Erlangen, FAU Erlangen-Nürnberg, Germany

**Abstract.** Despite their potential, markerless hand tracking technologies are not yet applied in practice to the diagnosis or monitoring of the activity in inflammatory musculoskeletal diseases. One reason is that the focus of most methods lies in the reconstruction of coarse, plausible poses for gesture recognition or AR/VR applications, whereas in the clinical context, accurate, interpretable, and reliable results are required. Therefore, we propose **ShaRPy**, the first RGB-D **Shape Reconstruction** and hand **Pose** tracking system, which provides uncertainty estimates of the computed pose to guide clinical decision-making. Our method requires only a light-weight setup with a single consumer-level RGB-D camera yet it is able to distinguish similar poses with only small joint angle deviations. This is achieved by combining a data-driven dense correspondence predictor with traditional energy minimization, optimizing for both, pose and hand shape parameters. We evaluate ShaRPy on a keypoint detection benchmark and show qualitative results on recordings of a patient.

**Keywords:** Inflammatory Musculoskeletal Diseases · Hand Pose and Shape Tracking · Uncertainty Estimation.

## 1 Introduction and Related Work

Hand function is affected by musculoskeletal rheumatic diseases. Rheumatoid Arthritis (RA) and Psoriatic Arthritis (PsA) are both common chronic inflammatory diseases, characterized by joint pain and swelling that can result in joint destruction [14]. In view of improved treatment options a more detailed, objective assessment of hand function is desirable, as it can potentially serve as a biomarker for changes in disease activity and patient quality of life [12]. This would allow for early therapy adjustment and potentially improve the prediction of increased risk of joint destruction. In clinical practice, functional assessments are mainly based on subjective questionnaires [21] or manual tests [8] that can

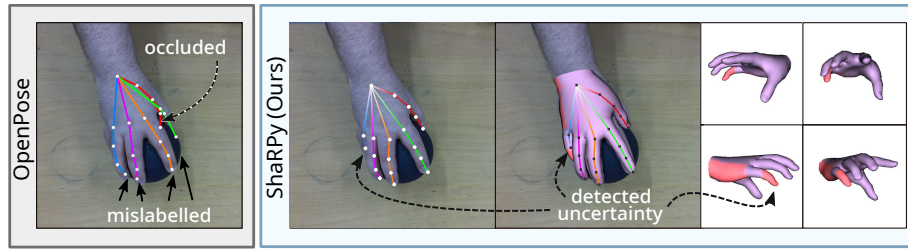


Fig. 1: Compared to keypoint approaches, e.g. OpenPose [2,23], ShaRPpy estimates the 3D hand pose and shape, and indicates uncertainty by detecting unobserved and error-prone regions (both visualized in red on the hand surface).

discriminate between healthy individuals and patients, but lack sensitivity for disease monitoring over time [20]. The gold standard for objective hand motion assessment is marker-based motion capturing [15]. Other methods use gloves and inertial measurement units [7,22] to record or monitor hand motion. A major drawback of these technologies is that they are contact-based, time-consuming to set up, and do not provide direct and intuitive visual feedback options. Hence, simple markerless camera-based hand movement assessments are desirable and show promising potential to be applied in the future [18].

In the computer vision community, camera-based hand reconstruction has a rich history [25]. Hand pose estimation algorithms usually reconstruct hands as a set of keypoints [29,5]. However, the visual interpretability of keypoints is limited (cf. Fig. 1) as they do not reflect shape and shape-dependent pose. For example, the neutral posture with all fingers closed of a thick hand is identical to a thin hand with a slight abduction in the Metacarpophalangeal (MCP) joints. Another line of work focuses on estimating the pose of parametric hand models including shape [11,27,4,17]. Commonly, a neural network [11,27] is trained, which is fixed at inference time and restricted in its generalization capability with respect to unseen shapes, poses, and viewpoints. Alternative approaches are based on energy optimization, e.g. [4,17], which can be adjusted to individual video sequences and extended to fit clinical requirements, e.g. including anthropometric hand constraints. The common goal of all the above approaches is to estimate the most plausible pose of the hand and its skeleton. However, in difficult cases (cf. Fig. 1), this means that the finger segments can be mislabelled, point into the wrong direction, or are speculated at positions that are not visible. In clinical setups, besides accuracy, it is important to identify and discard unreliable measurements and avoid false positives in the assessment of hand functions.

To tackle all these limitations, we propose, to the best of our knowledge, the first markerless hand tracking method, which provides accurate hand pose *and* shape parameters *and* estimates the uncertainty that remains in those in order to discard unreliable predictions. Our approach requires only a single RGB-D camera, which makes it easily applicable and allows us to determine a metrically accurate hand shape and pose.

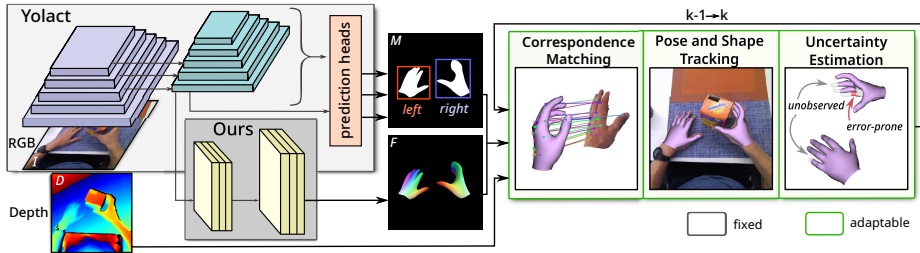


Fig. 2: Overview of ShaRPy. First, a network based on Yolact [1] detects hands and regresses features in a correspondence space. The outputs and the depth map are used in a subsequent energy minimization framework for pose and shape estimation. Lastly, we detect uncertainties with respect to the pose parameters.

## 2 Methods

An overview of ShaRPy is shown in Fig. 2. First, a pre-trained multi-task network [1] predicts for each hand in an RGB image  $\mathbf{I}$  its bounding box, a label indicating whether it is the left or right hand, a segmentation mask  $\mathbf{M}$ , and a correspondence image  $\mathbf{F}$  (Sec. 2.1). Next, the optimal pose and shape parameters of a parametric hand model are found in an energy minimization framework using the additional depth image  $\mathbf{D}$  (Sec. 2.2). Lastly, we estimate the uncertainty through the calculation of unobserved and error-prone regions (Sec. 2.2). Our tracking approach leverages the advantages of video data and reuses network and hand model predictions of the previous frame at timestep  $k - 1$ .

**Hand Model.** We employ the widely adopted MANO model [19] as a parametric representation of the hand. The model is represented by a set of vertices  $\mathcal{V} \subseteq \mathbb{R}^3$ , deformed by a kinematic tree of 15 finger joints  $\mathcal{J} \subseteq \mathbb{R}^3$ , and a root wrist joint. The rigid motion of the wrist is described by the translation vector  $\mathbf{t} \in \mathbb{R}^3$  and rotation  $\mathbf{R} \in \mathbb{R}^3$  in axis-angle notation. Similarly, the per-joint rotations are denoted as the pose  $\boldsymbol{\theta} \in \mathbb{R}^{3|\mathcal{J}|}$ , and the hand shape is parameterized by  $\boldsymbol{\beta} \in \mathbb{R}^{10}$ . A linear function maps the pose and shape parameters to joints and, subsequently, to vertices. As the model is not anatomically constrained, the orientation of the joints is not aligned with the natural bone structure. Together with the high number of 3 Degrees-of-Freedom (DoF) per joint, the parametrization can lead to unnatural poses. Inspired by [27], we rephrase the orientation of a per-joint pose such that the respective joint moves within the sagittal, coronal, and transverse plane. Furthermore, we propose to limit the DoF per joint with respect to anatomy considering the special case of the thumb. The MANO extension is shown in Fig. 3 and enables an anatomically correct pose parametrization  $\boldsymbol{\theta} \in \mathbb{R}^{23}$ .

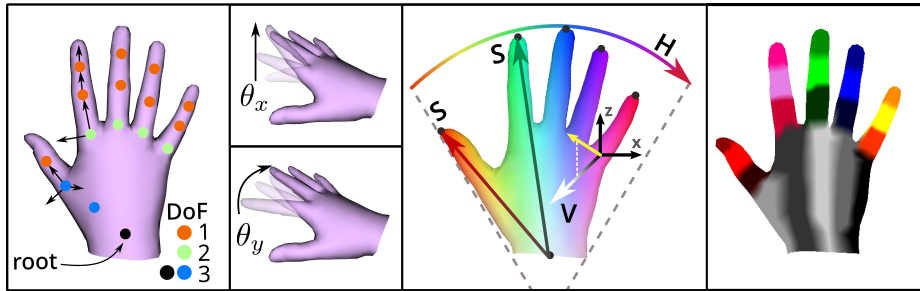


Fig. 3: Left: The anatomical MANO model with exemplary movements of joint  $i$  in the sagittal ( $\theta_x^i$ ) and coronal plane ( $\theta_y^i$ ). Middle: Dense correspondence encoding. Right: Segmentation sets  $S_{3d}^i$  computed from correspondence space.

## 2.1 Dense Correspondence with Semantic Encodings

Our goal is to fit the MANO model such that it best describes the observations in an RGB-D image. To this end, we establish correspondences between a pixel  $(x, y)$  and a vertex  $\mathbf{v} \in \mathcal{V}$  through a novel, shared canonical correspondence space embedded in  $[0, 1]^3$ . For this, we define the function  $\mathbf{c}: \mathcal{V} \rightarrow [0, 1]^3$ , which maps  $\mathbf{v}$  to its coordinate in the correspondence space. As depicted in Fig. 3, the space is encoded into a Hue-Saturation-Value (HSV) color cylinder wrapped around the flat rest pose of the model, aligned such that the axes describe semantic features of the hand. The hue range is scaled to lie within the extent of the MANO model and describes the finger type. The saturation is computed on each finger separately and encodes the corresponding segment. To distinguish between the front and back of the hand, the value axis encodes the surface normal along the  $y$ -axis. In summary, the correspondence space encodes both, spatial and semantic hand features while being compact, continuous, and deterministic to compute. The semantic encoding enables us to define a function  $d: [0, 1]^3 \rightarrow \{1, \dots, 20\}$  that computes a discrete segmentation label out of the continuous space, which is later used in Sec. 2.2. Fig. 3 shows the corresponding segmented vertex sets  $\mathcal{S}_{3d} = \{S_{3d}^i\}_{i=1}^{20}$  with  $S_{3d}^i = \{\mathbf{v} \in \mathcal{V} \mid d(\mathbf{c}(\mathbf{v})) = i\}$ , of which 15 refer to the three segments of each finger, and the remaining divide the large area of the wrist into 5 per-finger regions.

**Correspondence Regression.** As depth-only datasets are limited in availability and generalization across depth images of different sensor types is challenging, we leverage a variety of RGB(-D) datasets [16,28,9,4,5] to train our network only on RGB data in a fully supervised manner. We use a mixture of (semi-)automatically labeled ground-truth MANO parameters to transform the models to their position in the image and render the parts of the visible surface to obtain ground-truth correspondence images. The network is an extension of Yolact [1] with an additional branch for correspondence prediction, which is trained by minimizing the smooth L1 loss between the predicted and ground-truth correspondence value of each pixel within the ground-truth segmentation

mask of the hand. At inference time, we multiply the correspondence values with the predicted mask  $\mathbf{M}$  to acquire per-pixel correspondences only for the hand.

**Correspondence Matching.** Correspondence pairs are established by comparing each predicted  $\mathbf{c}_p = \mathbf{F}(x, y)$  at pixel  $(x, y)$  with  $\mathbf{c}_v = \mathbf{c}(\mathbf{v})$  of every MANO vertex  $\mathbf{v}$ . However, to find a match, using a traditional distance thresholded nearest-neighbor [17] algorithm is not the optimal strategy as the continuous nature of the correspondence space can lead to wrong assignments at positions in between fingers. Thus, we compute nearest-neighbor matches within each segmented vertex set  $\mathcal{S}_{3d}^i$  and its corresponding pixel set  $\mathcal{S}_{2d}^i = \{(x, y) \mid d(\mathbf{F}(x, y)) = i\}$  instead. A match between  $\mathbf{c}_p$  and  $\mathbf{c}_v$  is used to construct a pair  $(\mathbf{p}, \mathbf{v})$  of 3D correspondences between  $\mathbf{v}$  and an image point  $\mathbf{p} \in \mathbb{R}^3$ , computed from the back-projection of the depth value at  $\mathbf{D}(x, y)$ . Since  $\mathbf{c}_p$  is predicted in the view of the RGB camera, it is not exactly aligned with the pixel positions of  $\mathbf{D}$ . Particularly at the edges of the hand silhouette, the predictions can map to erroneous points of the background. Hence, we first discard pairs, in which  $\mathbf{D}(x, y)$  deviates too far from the median depth of the hand, determined by a threshold  $t_d$ . Second, we filter out points at silhouette edges with degraded and noisy depth by inspecting whether the angle of the point-wise normal computed from  $\mathbf{D}$  exceeds a given threshold  $t_n$ . Lastly, we discard all pairs  $(\mathbf{p}, \mathbf{v})$ , of which the Euclidean norm of their difference exceeds the 3D distance threshold  $t_{3d}$ . The final 3D correspondence set is denoted by  $\mathcal{C}_{3d}$ .

## 2.2 Pose and Shape Tracking with Uncertainty Estimation

In this stage, we solve an energy-minimization problem  $E$  to obtain the optimal MANO parameter set  $\Omega^k = (R^k, t^k, \theta^k, \beta^k)$  at timestep  $k$ :

$$\arg \min_{\Omega^k} E = \arg \min_{\Omega^k} [\omega_{3d} \lambda E_{3d}(\mathcal{C}_{3d}) + \omega_{2d} E_{2d}(\mathcal{C}_{2d}) + E_{reg}(\Omega^k, \Omega^{k-1})]$$

We denote the respective weights of a term  $E_*$  as  $\omega_*$  and define  $\lambda = \exp(J + 1)$ , where  $J$  is the Jaccard index of the predicted mask  $\mathbf{M}$  and the mask  $\mathbf{M}_v$  of the rasterized MANO model (by using Nvdiffrast [10]).  $E_{3d}$  and  $E_{reg}$  are similar to Mueller et al. [17]: The data term  $E_{3d}$  consists of a point-to-point and point-to-plane error. The regularization term  $E_{reg}$  enforces plausible poses and shapes, as well as temporal smoothness, and consists of  $E_{shape}$ ,  $E_{pose}$ , and  $E_{temp}$  [17]. We introduce the term  $E_{2d}$  defined on the set of valid pixels  $\mathcal{C}_{2d}$  within  $\mathbf{M}$  and  $\mathbf{M}_v$ . For each pixel  $(x, y) \in \mathcal{C}_{2d}$ , the term penalizes the squared L2 norm between  $\mathbf{F}(x, y)$  and  $\mathbf{F}_v(x, y)$ , where  $\mathbf{F}_v$  is the correspondence image of the rasterized MANO model. In other words,  $E_{2d}$  enforces MANO to lie within the predicted hand silhouette and provides a more accurate estimation of  $\beta$  compared to  $E_{3d}$ . In our energy minimization framework, we distinguish between the *Initialization* phase, which is only executed in the first frame or when the tracking is lost, and the *Refinement* phase, in which we iteratively minimize  $E$ . During initialization, we first solve the orthogonal Procrustes problem to obtain the initial wrist parameters  $\mathbf{R}$  and  $\mathbf{t}$ . Secondly, we make use of an implicit pose prior to initialize  $\theta$

with plausible parameters. For this purpose, we transform  $\theta$  into a PCA space pre-computed from annotated RGB(-D) datasets [16,28,9,4,5]. Then, we solve  $E$  with respect to the PCA pose parameters.

**Uncertainty Estimation.** At last, we compute an uncertainty value  $u_i$  for each segment  $i$  on the surface of the MANO model given by  $S_{3d}^i$  such that:

$$u_i = \begin{cases} 1 & \text{if segment } i \text{ unobserved or error-prone} \\ 0 & \text{else} \end{cases}$$

Since a segment relates to the set of vertices deformed by a particular joint, we can directly infer uncertainty with respect to its respective pose parameter. We consider a segment  $i$  as unobserved if:

$$\frac{|\mathcal{V}_{vis}^i|}{|S_{3d}^i|} < \tau_v, \quad \text{with } \mathcal{V}_{vis}^i = \{v \in S_{3d}^i \mid (*, v) \in C_{3d}\}$$

Further, we consider a segment  $i$  as error-prone if:

$$\frac{|\mathcal{P}_{2d}|}{|S_{2d}^i|} > \tau_{2d} \quad \text{or} \quad \frac{|\mathcal{P}_{3d}|}{|S_{3d}^i|} > \tau_{3d}$$

We define  $\mathcal{P}_{2d}^i = \{(x, y) \in S_{2d}^i \mid (x, y) \in C_{2d} \wedge E_{2d}(x, y) > \varepsilon_{2d}\}$  as the set of error-prone pixels and, analogously,  $\mathcal{P}_{3d}^i = \{\mathbf{v} \in S_{3d}^i \mid (*, \mathbf{v}) \in C_{3d} \wedge E_z(\mathbf{v}) > \varepsilon_{3d}\}$  as the set of error-prone vertices. The term  $E_z(\mathbf{v})$  is defined as the average L1 loss between the z-axis values of all pairs in  $C_{3d}$ , in which  $\mathbf{v}$  is included.

### 3 Results

Our network is implemented and trained in PyTorch. For the evaluation, we apply three different training procedures, denoted as  $V1$ ,  $V2$ , and  $V3$ . In  $V1$ , we exclusively train on the H2O [9] dataset. In  $V2$ , we train on all previously mentioned datasets [9,4,5,16,28]. In  $V3$ , we exclude H2O and train on the remaining data [4,5,16,28]. At inference time, the network is embedded together with the rest of the pipeline into a common C++ framework. During shape and pose estimation, we initialize the tracking by using libTorch’s L-BFGS optimizer and then iteratively refine the energy with Adam. The results are divided into two experiments. First, we show the clinical applicability of our setup on a male, 61 years old PsA patient (Disease Activity in Psoriatic Arthritis score: 17.52) and demonstrate the reliability to discard invalid pose predictions through the detection of uncertainty. Second, we quantitatively and qualitatively compare the accuracy of our method with the state-of-the-art (SOTA).

**Clinical applicability.** Similar to clinical practice, we recorded a sequence of the finger adduction and abduction together with the finger hyperextension and assess the hand function by measuring the angles of the fingers, using the middle

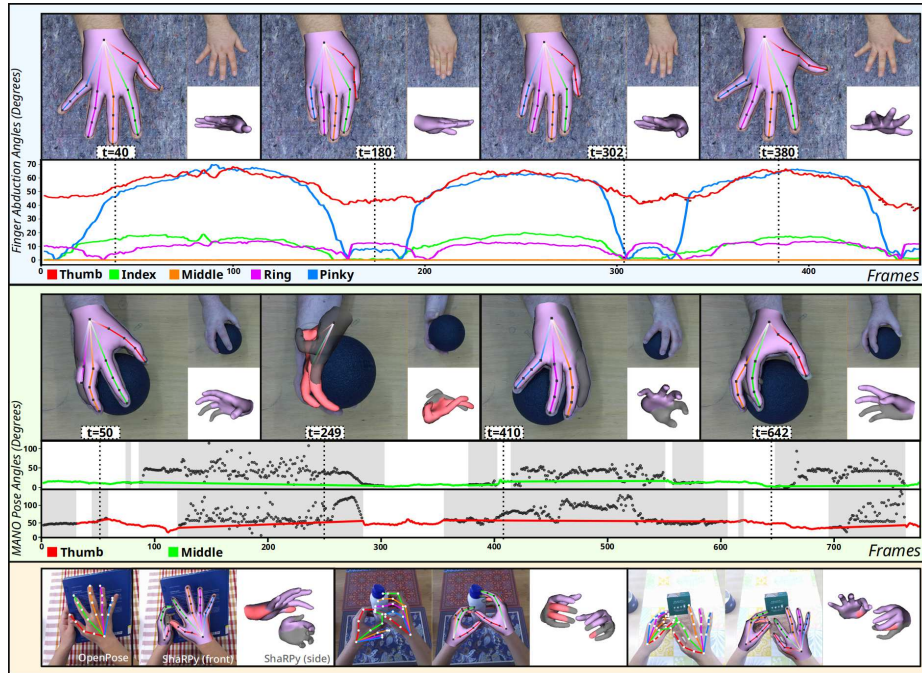


Fig. 4: Top: Images and angle results from an abduction and adduction sequence (repeated  $3\times$ ). Middle: Results of the rotating ball sequence. Unobserved (grey hand surface) or error-prone (red surface) poses are listed as disconnected grey dots in the plots. Bottom: Comparison of ShaRPy with OpenPose [2,23].

finger as a reference. We achieve this by projecting the segments between the proximal interphalangeal joints (PIP) and MCP joints onto the wrist plane and computing the angle deviation from the PIP-MCP segment of the middle finger. The results are depicted in Fig. 4. We are further able to visualize the finger hyperextension due to the depth information, which is not possible in RGB-only approaches. Next, we recorded the patient holding a ball and rotating the wrist around the camera. As we can assume that the fingers hardly move during this task, we expect corresponding results in the finger angles. We plot the angles of the pose  $\theta$  around the MCP of the thumb and the index and filter out all measurements, in which one of the respective finger segments is marked as uncertain within three consecutive frames. We compare the results with unfiltered angle measurements and perceive a significant decrease in angle variance from  $112.55^\circ$  to  $18.16^\circ$  on the middle finger and from  $125.29^\circ$  to  $37.84^\circ$  on the thumb, which was less visible and mainly close to silhouette edges in the depth map.

**Comparison with State-of-the-art.** Since there is no established evaluation method for *dense* pose and *shape* estimation with *uncertainty* estimation in *clinical* applications, we compare our method with the SOTA on pose estima-

	MEPE (mm)↓		3D PCK@15mm↑		3D PCK@30mm↑	
	left	right	left	right	left	right
Cho et al. [3]*	14.40	15.90	70.75	54.61	93.81	95.08
Luo et al. [13]*	20.80	24.70	40.77	32.29	80.36	73.56
Wen et al. [26]*	35.00	35.60	12.67	2.98	43.71	37.12
Hasson et al. [6]	39.56	41.87	-	-	-	-
Tekin et al. [24]	41.32	38.86	-	-	-	-
Kwon et al. [9]	41.45	37.21	-	-	-	-
<b>Ours (V1)</b>	20.47	19.07	21.04	27.81	92.81	94.73
<b>Ours (V3)</b>	28.62	28.42	12.95	16.64	81.61	86.15

Table 1: Results on the H2O [9] hand pose challenge. Workshop contributions, particularly focused on the H2O challenge, are denoted as (·)\*.

tion. Therefore, we evaluate the accuracy of ShaRPy on the H2O [9] dataset, which contains egocentric RGB-D sequences of healthy subjects most visually close to a clinical setting. In Fig. 4, we compare our qualitative results on V2 with OpenPose [2,23]. For a quantitative comparison, our results are submitted and objectively evaluated on a public leaderboard<sup>4</sup>. The benchmark is tailored to RGB keypoint-based methods and evaluates the plausibility of poses in the presence of strong occlusions. Tab. 1 summarizes the results with respect to the Mean End-point Error (MEPE) and the Percentage of Correct Keypoints (PCK). In summary, ShaRPy places second or third on the leaderboard, even though we did not design our system specifically for a keypoint-based pose estimation challenge (as compared to [3,13,26]), do not focus on plausibility, and, solve a more challenging problem of indirectly estimating the pose through shape along with the shape itself. On top of that, we show the generalization ability of our version V3, which outperforms most methods by placing third.

**Conclusion.** In this work, we proposed the first markerless hand tracking approach, which calculates uncertainty in the pose estimates. Our approach combines a data-driven dense correspondence predictor with a flexible, generative energy minimization framework to estimate the optimal hand pose and shape that best explains the given observations. Further, we detect uncertain poses through the detection of unobserved and error-prone surface segments. We demonstrate through quantitative and qualitative results that our approach provides outstanding pose estimation accuracy, on top of its generalization to both, unknown datasets of healthy individuals and patient data. Furthermore, we provide results of clinical hand function assessments and show that, compared to other markerless approaches, our approach has no limitation in terms of its applicability and, instead, includes more favorable properties such as additional shape estimation and the robust filtering of uncertain poses. We believe our approach can be used to drive further research in the context of markerless

<sup>4</sup> <https://codalab.lisn.upsaclay.fr/competitions/4822>

tracking in clinical applications.

**Data Use Declaration and Acknowledgments.** We thank **Maximilian Weiherer** for his valuable feedback. The protocol was approved by the FAU ethics committee (*357\_20B*). Patient data was recorded after given written informed consent. This work was funded by the Deutsche Forschungsgemeinschaft (DFG, German Research Foundation) – SFB 1483 – Project-ID 442419336, EmpkinS. This work used the German Research Foundation (DFG) funded major instrument (reference number INST90 / 985-1 FUGG) at the Institute of Applied Dynamics (Sigrid Leyendecker), Friedrich-Alexander Universität Erlangen-Nürnberg Germany. The authors gratefully acknowledge the scientific support and HPC resources provided by the Erlangen National High Performance Computing Center of the Friedrich-Alexander-Universität Erlangen-Nürnberg.

## References

1. Bolya, D., Zhou, C., Xiao, F., Lee, Y.J.: Yolact: Real-time instance segmentation. In: ICCV (2019)
2. Cao, Z., Hidalgo Martinez, G., Simon, T., Wei, S., Sheikh, Y.A.: Openpose: Real-time multi-person 2d pose estimation using part affinity fields. *IEEE Transactions on Pattern Analysis and Machine Intelligence* (2019)
3. Cho, H., Kim, D., Kim, C., Lee, S., Baek, S.: Transformer-based Global 3D Hand Pose Estimation in Two Hands Manipulating Objects Scenarios. arXiv e-prints arXiv:2210.11384 (Oct 2022). <https://doi.org/10.48550/arXiv.2210.11384>
4. Hampali, S., Rad, M., Oberweger, M., Lepetit, V.: Honnotate: A method for 3d annotation of hand and object poses. In: CVPR (2020)
5. Hampali, S., Sarkar, S.D., Rad, M., Lepetit, V.: Keypoint transformer: Solving joint identification in challenging hands and object interactions for accurate 3d pose estimation. In: 2022 IEEE/CVF Conference on Computer Vision and Pattern Recognition (CVPR). pp. 11080–11090 (2022). <https://doi.org/10.1109/CVPR52688.2022.01081>
6. Hasson, Y., Tekin, B., Bogo, F., Laptev, I., Pollefeys, M., Schmid, C.: Leveraging photometric consistency over time for sparsely supervised hand-object reconstruction. *CoRR* **abs/2004.13449** (2020), <https://arxiv.org/abs/2004.13449>
7. Henderson, J., Condell, J., Connolly, J., Kelly, D., Curran, K.: Review of Wearable Sensor-Based Health Monitoring Glove Devices for Rheumatoid Arthritis. *Sensors (Basel)* **21**(5) (2021). <https://doi.org/doi:10.3390/s21051576>
8. Higgins, S.C., Adams, J., Hughes, R.: Measuring hand grip strength in rheumatoid arthritis. *Rheumatol International* **38**(5), 707–714 (2018). <https://doi.org/doi:10.1007/s00296-018-4024-2>
9. Kwon, T., Tekin, B., Stühmer, J., Bogo, F., Pollefeys, M.: H2o: Two hands manipulating objects for first person interaction recognition. In: Proceedings of the IEEE/CVF International Conference on Computer Vision (ICCV). pp. 10138–10148 (October 2021)
10. Laine, S., Hellsten, J., Karras, T., Seol, Y., Lehtinen, J., Aila, T.: Modular primitives for high-performance differentiable rendering. *ACM Transactions on Graphics* **39**(6) (2020)

11. Lin, K., Wang, L., Liu, Z.: End-to-end human pose and mesh reconstruction with transformers. In: CVPR (2021)
12. Liphardt, A.M., Manger, E., Liehr, S., Bieniek, L., Kleyer, A., Simon, D., Taskilar, K., Sticherling, M., Rech, J., Schett, G., Hueber, A.J.: Similar Impact of Psoriatic Arthritis and Rheumatoid Arthritis on Objective and Subjective Parameters of Hand Function. *ACR Open Rheumatology* **2**(12), 734–740 (2020). <https://doi.org/doi:10.1002/acr2.11196>
13. Luo, W., Cao, S., Wang, B., Zhang, W., Wei, X., Ma, L.: Yolov7-3d: One-stage monocular 3d hand pose estimation. In: 2022 IEEE International Conference on Computer Vision (ICCV) Workshops: Human Body, Hands, and Activities from Egocentric and Multi-view Cameras (HBHA) (2022)
14. Merola, J.F., R, E.L., Roy, F.: Distinguishing rheumatoid arthritis from psoriatic arthritis. *RMD Open* (2018). <https://doi.org/doi:10.1136/rmdopen-2018-0006565>
15. Metcalf, C.D., Notley, S.V., Chappell, P.H., Burridge, J.H., Yule, V.T.: Validation and application of a computational model for wrist and hand movements using surface markers. *IEEE Trans Biomed Eng* **55**(3), 1199–1210 (2008). <https://doi.org/doi:10.1109/TBME.2007.908087>
16. Moon, G., Yu, S.I., Wen, H., Shiratori, T., Lee, K.M.: Interhand2.6m: A dataset and baseline for 3d interacting hand pose estimation from a single rgb image. In: European Conference on Computer Vision (ECCV) (2020)
17. Mueller, F., Davis, M., Bernard, F., Sotnychenko, O., Verschoor, M., Otaduy, M.A., Casas, D., Theobalt, C.: Real-time Pose and Shape Reconstruction of Two Interacting Hands With a Single Depth Camera. *ACM Transactions on Graphics (TOG)* **38**(4) (2019)
18. Phutane, U., Liphardt, A.M., Bräunig, J., Penner, J., Klebl, M., Tascilar, K., Vossiek, M., Kleyer, A., Schett, G., Leyendecker, S.: Evaluation of Optical and Radar Based Motion Capturing Technologies for Characterizing Hand Movement in Rheumatoid Arthritis-A Pilot Study. *Sensors (Basel)* **21**(4) (2021). <https://doi.org/doi:10.3390/s21041208>
19. Romero, J., Tzionas, D., Black, M.J.: Embodied hands: Modeling and capturing hands and bodies together. *ACM Transactions on Graphics, (Proc. SIGGRAPH Asia)* **36**(6) (Nov 2017)
20. Rydholm, M., Wikström, I., Hagel, S., Jacobsson, L.T.H., Turesson, C.: The Relation Between Disease Activity, Patient-Reported Outcomes, and Grip Force Over Time in Early Rheumatoid Arthritis. *ACR Open Rheumatology* **1**(8), 507–515 (2019). <https://doi.org/doi:10.1002/acr2.11062>
21. Salaffi, F., Di Carlo, M., Farah, S., Marotto, D., Atzeni, F., Sarzi-Puttini, P.: Rheumatoid Arthritis disease activity assessment in routine care: performance of the most widely used composite disease activity indices and patient-reported outcome measures. *ACR Open Rheumatology* **92**(4) (2021). <https://doi.org/doi:10.23750/abm.v92i4.10831>
22. Salchow-Hömmen, C., Callies, L., Laidig, D., Valtin, M., Schauer, T., Seel, T.: A Tangible Solution for Hand Motion Tracking in Clinical Applications. *Sensors (Basel)* **19**(1), 1199–1210 (2019). <https://doi.org/doi:10.3390/s19010208>
23. Simon, T., Joo, H., Matthews, I., Sheikh, Y.: Hand keypoint detection in single images using multiview bootstrapping. In: CVPR (2017)
24. Tekin, B., Bogo, F., Pollefeys, M.: H+o: Unified egocentric recognition of 3d hand-object poses and interactions. In: 2019 IEEE/CVF Conference on Computer Vision and Pattern Recognition (CVPR). pp. 4506–4515 (2019). <https://doi.org/10.1109/CVPR.2019.00464>

25. Tretschk, E., Kairanda, N., R, M.B., Dabral, R., Kortylewski, A., Egger, B., Habermann, M., Fua, P., Theobalt, C., Golyanik, V.: State of the art in dense monocular non-rigid 3d reconstruction (2022), <https://arxiv.org/abs/2210.15664>
26. Wen, Y., Pan, H., Yang, L., Pan, J., Komura, T., Wang, W.: Hierarchical Temporal Transformer for 3D Hand Pose Estimation and Action Recognition from Egocentric RGB Videos. arXiv e-prints arXiv:2209.09484 (Sep 2022). <https://doi.org/10.48550/arXiv.2209.09484>
27. Yang, L., Zhan, X., Li, K., Xu, W., Li, J., Lu, C.: Cpf: Learning a contact potential field to model the hand-object interaction. In: 2021 IEEE/CVF International Conference on Computer Vision (ICCV). pp. 11077–11086 (2021). <https://doi.org/10.1109/ICCV48922.2021.01091>
28. Zimmermann, C., Argus, M., Brox, T.: Contrastive representation learning for hand shape estimation. In: Bauckhage, C., Gall, J., Schwing, A. (eds.) Pattern Recognition. pp. 250–264. Springer International Publishing, Cham (2021)
29. Zimmermann, C., Brox, T.: Learning to estimate 3d hand pose from single rgb images. In: 2017 IEEE International Conference on Computer Vision (ICCV). pp. 4913–4921 (2017). <https://doi.org/10.1109/ICCV.2017.525>